IEEE Access
Multidisciplinary ⋮ Rapid Review ⋮ Open Access Journal

Received January 5, 2020, accepted January 15, 2020, date of publication January 17, 2020, date of current version January 28, 2020.

Digital Object Identifier 10.1109/ACCESS.2020.2967563

Comparative Study of the Influence of Open Circuit Voltage Tests on State of Charge Online Estimation for Lithium-Ion Batteries

YUAN LI[1, 2], HAO GUO[3], (Member, IEEE), FEI QI[4], (Member, IEEE), ZHIPING GUO[5], AND MEIYING LI[5]

[1]College of Energy and Power Engineering, Inner Mongolia University of Technology, Hohhot 010050, China
[2]School of Electrical Engineering and Computer Science, KTH Royal Institute of Technology, 10044 Stockholm, Sweden
[3]Jiangsu Provincial Key Laboratory of Advanced Robotics, Robotics and Microsystems Center, Soochow University, Suzhou 215021, China
[4]School of Mechanical and Electric Engineering, Soochow University, Suzhou 215021, China
[5]College of Mechanical Engineering, Inner Mongolia University of Technology, Hohhot 010050, China

Corresponding author: Zhiping Guo (121375322@qq.com)

This work was supported in part by the Major Program of Natural Science Foundation of Inner Mongolia under Grant 2017ZD02, and in part by the National Natural Science Foundation of China under Grant 11402156 and Grant 61503269.

ABSTRACT The accurate state of charge (SoC) online estimation is a significant indicator that relates to driving ranges of electric vehicles (EV). The relationship between open circuit voltage (OCV) and SoC plays an important role in SoC estimation for lithium-ion batteries. To compare with the traditional incremental OCV (IO) test and the low current OCV (LO) test, a novel OCV test which combines IO test with LO test (CIL) is proposed in this paper. Based on the reliable parameters online identification of the dual polarization (DP) battery model, two SoC estimation algorithms are compared on the accuracy, robustness and convergence speed for the entire SoC region. Meanwhile, the comparative study of the three OCV-SoC relationships fits by the corresponding OCV tests is discussed in terms of the SoC online estimation under various temperatures. The results show that the adaptive extended Kalman filter (AEKF) algorithm can better improve the accuracy and robustness of SoC estimation than that of the extended Kalman filter (EKF) algorithm. Most importantly, the OCV-SoC relationship obtains from the CIL OCV test method is applied to the AEKF algorithm, which has higher accuracy and better statistical indices of SoC estimation, especially suitable for the low temperature.

INDEX TERMS Lithium-ion batteries, state of charge estimation, open circuit voltage test, online parameters identification, adaptive extended Kalman filter algorithm.

I. INTRODUCTION

With the development of the automobile manufacturing industry towards to the tendency of the cleanliness, efficiency and sustainability, the EV is the most potential choice to solve the above problems, which has made great progress and development in the industrial and commercial fields [1], [2]. Lithium-ion batteries with the high energy density and the long cycle life are commonly employed to supply energy for EVs [3]. Unfortunately, lithium-ion batteries cannot satisfy the requirement of the information transmission, control and management. Therefore, a battery management system (BMS) is developed to realize above-mentioned functions, which is responsible for monitoring the state of the battery, controlling the charge and discharge of the battery, and interacting the state information of the battery with the motor driver and the whole vehicle controller [4]–[6]. The battery SoC estimation is an essential ingredient of the BMS, which is approximately equivalent to the fuel gauge of the EV to indicate remaining driving ranges. Furthermore, the accurate SoC estimation also can provide a security assurance to the user due to it can avoid over-charge and over-discharge of lithium-ion batteries [7]. The mechanism of electrochemical reaction in the lithium-ion battery is difficult to determine, and the driving condition of the EV is complex, so it still needs explore to provide an accurate SoC estimation for the EV.

The coulomb counting method [8] and the open circuit voltage method [9] are widely used to the SoC estimation

The associate editor coordinating the review of this manuscript and approving it for publication was Zhen Li.

in the last few decades, because they have the characteristics of the simple principle and the less computational effort for the vehicle-mounted BMS system. However, it is difficult to meet with the complex and changeable driving conditions of EVs, due to its low accuracy and poor robustness of the SoC estimation results, so they are now replaced by other methods. The data-driven method as a new type of machine learning algorithm to achieve the SoC estimation in recent literatures [10], [11], which trains lots of experimental data to form the direct mapping relationship between the SoC and the current, voltage and temperature of the battery. Although the data-driven method can satisfy the accuracy of the SoC estimation for the nonlinear battery system, its accuracy and robustness strongly depend on the high algorithm complexity and plenty of training experimental data, which make it difficult to match well with the fast responsive BMS. The reality suggests most commonly accepted SoC estimation method for the BMS is the model-based method, which is a synthesis of the coulomb counting method and the open circuit voltage method by using the battery model and the state estimation algorithm [12]. The commonly used lithium-ion battery models include the electrochemical model [13], [14] and the equivalent circuit model (ECM) [15], [16] that both can describe the performance of the battery. Compared with the ECM model, complex partial differential equations and abundant electrochemical parameters of the electrochemical model are difficult to run and identify in the BMS, so the ECM model with the simple structure and a few parameters is selected to play an important role in the model-based method. The parameters identification of the ECM model is the top priority for the SoC estimation via the model-based method. The least square (LS) approach [17] and recursive least square (RLS) approach [18] are usually employed to identify parameters of the ECM model. Then the mapping relationship between the characteristic parameter of the ECM model and the SoC is established, which can be applied to the state estimation algorithm (such as the EKF algorithm [19], the particle filter algorithm [20], the dual EKF algorithm [21], the adaptive EKF algorithm [22] and other filter algorithm, etc. [23]) to correct the SoC estimation results of the coulomb counting method through the algorithm iterations. The SoC estimation results of the model-based method is determined by the battery model and the state estimation algorithm, which results in most literatures concentrate on how to improve the structure of the battery model and select the optimal filter algorithm to get an excellent SoC estimation with the high accuracy and the strong robustness. However, the common usage of the OCV-SoC mapping relationship acts as the interface channel between the battery model and the state estimation algorithm, whether it has an effect on the SoC estimation results of the model-based method is seldom discussed in literatures.

Widely adoptive the OCV tests are the low current OCV (LO) test and the incremental OCV (IO) test, which can respectively obtain the different OCV-SoC mapping relationships and result in different influences on the SoC estimation. Zheng *et al.* [24] conduct a comparative research about the influence of the LO test and the IO test on the SoC estimation at three dynamic tests under various temperatures, the study reveals that the SoC estimation results through the IO test performs better than that of the LO test. However, there have several imperfections need to be investigated and improved. Firstly, the OCV-SoC mapping relationship is developed via the offline lookup table, which will slow the running speed of the SoC estimation algorithm. Secondly, the parameters of the battery model are only identified from the dynamic stress test (DST) via LS approach under certain temperature, and then the parameters are applied to the filter algorithm to verify the accuracy of the SoC estimation by using other three driving tests under different temperatures, so it will lead to large SoC estimation errors, because the parameters identification comes from the DST test under certain temperature, which may not be generalizable for other driving tests. Lastly, the SoC estimation region is only occurred between 10% and 90%, which lacks of general applicability for the whole driving cycle of the EV. Lin *et al.* [25] also carry out a study about the impact of the LO test and the IO test on the SoC estimation and make corresponding modifications in terms of the above-mentioned imperfections of the study. But there still have seldom issues need to be investigated, such as the SoC estimation algorithm is verified by using the DST test. Compared with the real working condition of the EV, the DST is relatively easier than other dynamic tests. Thus, the results of this SoC estimation algorithm do not have universality for the complex test. Moreover, in order to improve the accuracy of the SoC estimation at low temperature, a method by adding relaxation time of the IO test is proposed, which can indirectly change the OCV-SoC mapping relationship. However, it will extend the test time and may result in failing to promote in the practice. Therefore, a detailed comparative analysis of different OCV tests for impact on the SoC estimation should be further researched.

The main contributions of this paper are as follows: (1) the paper innovatively proposed a novel OCV test method which combines incremental with low current OCV test; (2) the comparative investigations between the mapping relationship obtains from the novel OCV test and other OCV tests are done to explore the influence rule of the SoC estimation. (3) a recommended method in terms of the SoC estimation is given, especially suitable for the low temperature.

II. BATTERY MODEL

A. EQUIVALENT CIRCUIT MODEL OF THE BATTERY

The embedded system is commonly used to the BMS of the EV, which has limitations of the computing capacity and the memory space. Thus, it is important for selecting a battery model to represent the relationship between output characteristics of the battery and internal parameters. The fresh $LiFePO_4$ (LFP) battery is used in this paper and its detailed information is listed in Table 1. For the model selection, the dual polarization (DP) model is a 2-RC ECM to

TABLE 1. Detailed information of the fresh LFP battery.

Type	Nominal voltage	Nominal capacity	Upper/lower cut-off voltage	Maximum current
Pouch LFP	3.2 V	5.0 Ah	3.65 V/ 2.2 V	50 A (at 25° C)

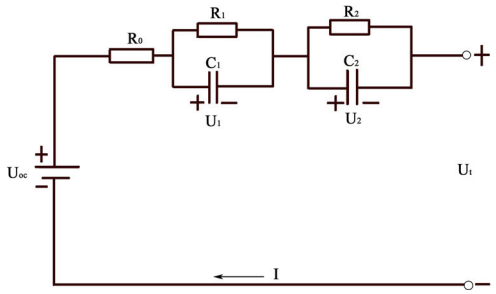

FIGURE 1. Dual polarization network structure model.

be employed in this paper, as shown in Fig.1, which has the better accuracy to describe the external characteristic of the battery than 1-RC model [26]. In the Fig.1, the DP model consists of three components, respectively are the voltage source and the ohmic resistance as well as the RC network, which has an excellent applicability at various operative modes for the battery. According to the Kirchhoff voltage law and the Kirchhoff current law, we can deduce the state-space equation to analyze and apply in the SoC estimation. The state-space equation of the battery can be expressed by the Eq. (1).

$$\begin{cases} \dot{U}_1 = \dfrac{I}{C_1} - \dfrac{U_1}{R_1 C_1} \\ \dot{U}_2 = \dfrac{I}{C_2} - \dfrac{U_2}{R_2 C_2} \\ U_t = U_{oc} - U_1 - U_2 - IR_0 \end{cases} \tag{1}$$

where U_{oc} denotes the open circuit voltage (OCV), R_0 is the ohmic resistance that represents the contact resistance between the electrode material and the electrolyte, *RC* network has two parts with the parallel structure of the resistance and the capacitance, which describes the dynamic performance of the battery along with polarization characteristics and diffusive effects. R_1, C_1 and R_2, C_2 are proposed to reveal the concentration polarization and the electrochemical polarization, respectively. U_1 and U_2 are polarization voltages that respectively across C_1 and C_2. U_t is the terminal voltage which can be directly measured. I is the current with the positive value or the negative value, which respectively represents the discharged process and the charged process.

In Eq. (2), we can fit the OCV-SoC relationship by using OCV-SoC test. Yu *et al.* [27] conduct an investigation about the sensitivities of OCV models to ambient temperatures, aging stages, numbers of data points, and SoC regions of LFP battery. According to his results, the 9th order polynomial model is the recommended choice for the LFP battery to describe the function relationship between OCV and SoC.

$$\begin{aligned} OCV = {} & k_0 + k_1 SoC + k_2 SoC^2 + k_3 SoC^3 + k_4 SoC^4 + k_5 SoC^5 \\ & + k_6 SoC^6 + k_7 SoC^7 + k_8 SoC^8 + k_9 SoC^9 \end{aligned} \tag{2}$$

where k_p $(p = 0, 1, \ldots, 9)$ are the coefficients of the polynomial function that used to fit the OCV-SoC relationship.

B. ONLINE IDETIFICATION OF THE BATTERY MODEL PARAMETERS

The online identification algorithm is a method that utilizes the real-time measured current, voltage and temperature to realize the online update of the battery model parameters. For the online parameter identification, we need to obtain the dispersed recursive expression of the DP battery model. Thus, Eq. (1) is transformed and then deduced the frequency-domain expression of the DP battery model, as shown in Eq. (3).

$$U_t(s) - U_{oc}(s) = -I(s)\left(R_0 + \frac{R_1}{1 + R_1 C_1 s} + \frac{R_2}{1 + R_2 C_2 s}\right) \tag{3}$$

where s is the frequency operator.

The corresponding transfer function of Eq. (3) is:

$$G(s) = -\frac{R_0 s^2 + \frac{R_0 R_1 C_1 + R_0 R_2 C_2 + R_2 R_1 C_1 + R_1 R_2 C_2}{R_1 C_1 R_2 C_2} s + \frac{R_0 + R_1 + R_2}{R_1 C_1 R_2 C_2}}{s^2 + \frac{R_1 C_1 + R_2 C_2}{R_1 C_1 R_2 C_2} s + \frac{1}{R_1 C_1 R_2 C_2}} \tag{4}$$

The Eq. (5) is a bilinear transform method that is used for the discretization calculation of Eq. (4) and the consequence is presented in Eq. (6),

$$s = \frac{2}{T} \cdot \frac{1 - z^{-1}}{1 + z^{-1}} \tag{5}$$

where the z is discretization operator.

$$G\left(z^{-1}\right) = \frac{w_3 + w_4 z^{-1} + w_5 z^{-2}}{1 - w_1 z^{-1} - w_2 z^{-2}} \tag{6}$$

where w_1, w_2, w_3, w_4, w_5 are the coefficients and which can be solved by Eq. (4).

A discretization form of Eq. (3) is rewritten as Eq. (7), where $k = 2, 3, 4 \ldots$,

$$\begin{aligned} U_t(k) = {} & 7\,(1 - w_1 - w_2)\,U_{oc}\,(k) + w_1 U_t\,(k-1) + w_2 U_t\,(k-2) \\ & + w_3 I(k) + w_4 I(k-1) + w_5 I(k-2) \end{aligned} \tag{7}$$

Definition:

$$\begin{aligned} \varphi(k) &= [1\ U_t(k-1)\ U_t(k-2)\ I(k)\ I(k-1)\ I(k-2)], \\ y_k &= U_t(k), \\ \theta(k) &= [(1 - w_1 - w_2) U_{oc}\ w_1\ w_2\ w_3\ w_4\ w_5]^T, \end{aligned}$$

Then

$$y_k = \varphi(k)\theta(k) \tag{8}$$

where I(k) can measure via the current sensor, θ(k) is the parameter vector to be identified, φ(k) is the input vector.

Due to the model parameters are susceptible to environmental changes, therefore it is difficult for the RLS approach to obtain the stable and reliable parameter identification results [28]. To resolve the problem in this paper, the RLS with an optimal forgetting factor (FRLS) is adopted to adjust data weight between old data and recent data, which enables the algorithm respond quickly and converge to the real value [29]. Thus,

$$\bar{\theta}(k) = \bar{\theta}(k-1) + P(k)\varphi(k)\left[y_k - \varphi^T(k)\bar{\theta}(k-1)\right] \quad (9)$$

where $\bar{\theta}(1) = \bar{\theta}(2) = \ldots\bar{\theta}(k) = \theta_0$

where θ_0 is a given initial value of parameter vector, and $P(k)$ is the gain factor, which is updated by

$$P(k) = \frac{1}{\lambda}\left[P(k-1) - \frac{P(k-1)\varphi(k)\varphi^T(k)P(k-1)}{\lambda + \varphi^T(k)P(k-1)\varphi(k)}\right] \quad (10)$$

where $P(1) = P(2) = \cdots = P(k) = p_0 E$

where p_0 is a large positive number, E is an identify matrix, and λ is the forgetting factor which value in this paper is 0.98.

With the updated $\varphi(k)$, the FRLS algorithm is realized, and the model parameters can be achieved by Eq. (11).

$$\begin{cases} R_0 = \dfrac{-w_3 + w_4 - w_5}{1 + w_1 - w_2} \\ R_1C_1R_2C_2 = \dfrac{-w_3 + w_4 - w_5}{1 - w_1 - w_2} \\ R_1C_1 + R_2C_2 = \dfrac{T(1 + w_2)}{1 - w_1 - w_2} \\ R_0 + R_1 + R_2 = \dfrac{-w_3 + w_4 - w_5}{1 - w_1 - w_2} \\ R_0R_1C_1 + R_0R_2C_2 + R_2R_1C_1 + R_1R_2C_2 = \dfrac{4(w_5 - w_3)}{T(1 + w_1 - w_2)} \end{cases} \quad (11)$$

III. OCV-SoC MAPPING TESTS

There is a monotonous mapping relationship between the OCV and the SoC. As we mentioned in the Eq. (2), the OCV-SoC mapping relationship has a crucial significance for improving the accuracy of the battery model and the SoC estimation [30]. For the SoC, we can calculate it by using ampere hour counting method, as shown in Eq. (12). Next section will indicate statements about the experiment of the OCV test and three methods of the OCV test.

$$y(t) = y(t_0) - \frac{\int_{t_0}^{t} \eta_i \cdot i(\tau)d\tau}{C_{\max}} \quad (12)$$

where $y(t)$ denotes the estimated value of SoC at t moment, $y(t_0)$ represents the initial value of SoC, η_i is the Coulombic efficiency during the charge process or discharge process, $i(\tau)$ is the current for the charge or discharge at τ moment, C_{max} represents the maximal capacity of the battery.

A. EXPERIMENT SETUP

In order to accomplish the OCV test, we build the battery testing platform that is shown in Fig.2. The platform consists of the control computer, the Neware battery testing system, and the thermal chamber. The control computer transfers testing orders by using the Neware software to the Neware battery testing system, which can conduct various battery tests. Properly drawn testing data are the voltage, current, temperature and capacity, etc. All the sampling frequency of the testing data is 1 Hz. Meanwhile, the testing battery commonly puts into the thermal chamber that can maintain stationary environment temperature. We separately conduct three methods of the OCV on the battery platform at 5°C, 25°C, and 40°C.

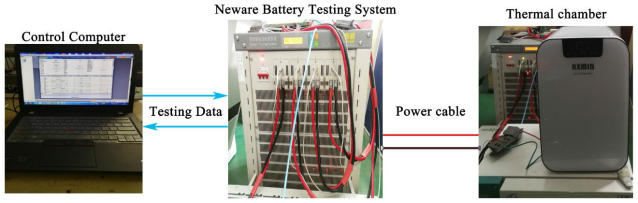

FIGURE 2. Battery testing platform.

B. LOW CURRENT OCV TEST

A constant low current of 0.05 C is adopted during the low current OCV test, and the testing terminal condition is the upper cut-off voltage reaches 3.65 V or lower cut-off voltage arrives 2.2V during the charged process or the discharged process. Fig.3(a)-(i) and (ii) respectively demonstrates the charged profile and discharged profile of the low current test about the LFP battery at 25°C. The terminal voltage approximately equals to the OCV at low current rate due to the low current reduces the concentration polarization and the electrochemical polarization effects inside the battery [31]. Thus, we can respectively fit OCV-SoC polynomial function through Eq. (2) using the terminal voltage data of the low current test at every 5% SoC of the charged and discharged processes.

C. INCREMENTAL OCV TEST

Before the incremental OCV test, the CCCV (constant current constant voltage) charged method is employed to make sure the battery is fully charged to 100% SoC. Then, ten current-relaxation durations with the negative pulse are applied to the battery, which is gradually discharged to 0% SoC. Every negative current-relaxation duration makes sure that the battery discharges 10% SoC. Meanwhile, the negative pulse current is 0.3 C and the relaxation time is 2 h that can minimize the concentration polarization and the electrochemical polarization effects inside the battery. After standing about 2 h, the battery is gradually charged using above the same scheme with the positive pulse to 100% SoC. The charged and discharged profiles of incremental OCV test at 25°C is displayed in Fig.3(b). Finally, we can respectively fit OCV-SoC polynomial function via Eq. (2) using the OCV voltage data of the incremental test at every 10% SoC of the charged and discharged processes.

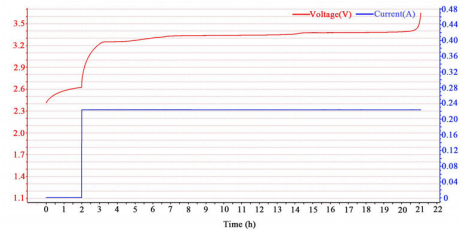

(i) charged profile

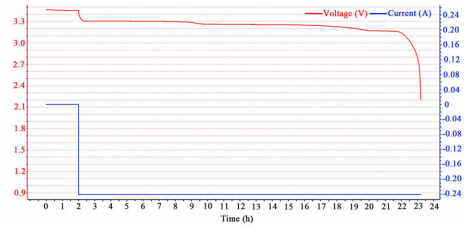

(ii) discharged profile

(a) Charged and discharged profiles of low current OCV test.

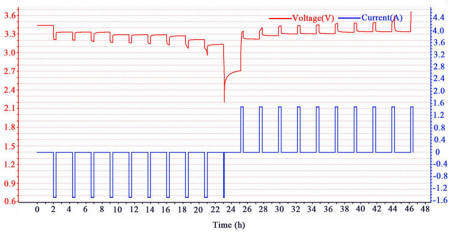

(b) Charged and discharged profiles of incremental OCV test.

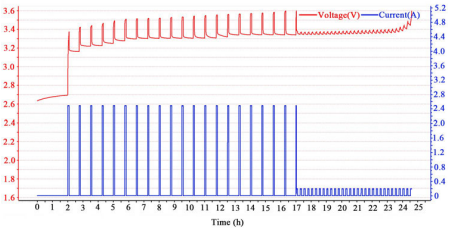

(i) charged profile

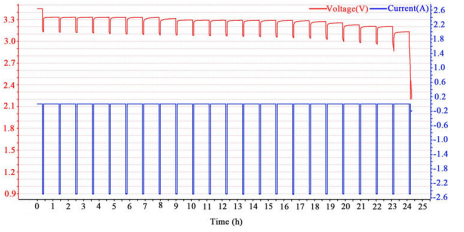

(ii) discharged profile

(c) Charged and discharged profiles of OCV test which combines incremental current with low current

FIGURE 3. Charged and discharged profiles of different OCV tests under 25°C.

D. COMBINED INCREMENTAL WITH LOW CURRENT OCV TEST

As stated above, the low current OCV test and the incremental OCV test are two OCV test methods, which are widely adopted for OCV-SoC mapping tests. A creative method which combines incremental with low current OCV test is used in this paper to conduct the OCV-SoC mapping test.

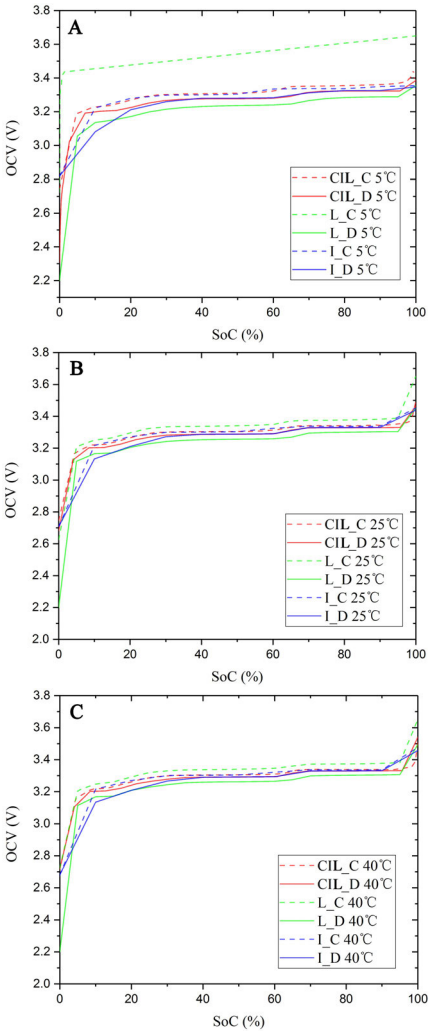

FIGURE 4. OCV-SoC curves of three tests at different temperatures: (A) 5°C, (B) 25°C, (C) 40°C.

The detailed charged testing schemes are: **a).** the C-rate of the battery is 0.5 C with CC charged method for 300 s, if the terminal voltage is greater than the cut-off voltage 3.65 V, the testing procedure goes to **c)**, else goes to **b)**; **b)**. rest for 3600 s, then go to **a)**; **c).** low current with 0.04 C that continuously charges 300 s, if the terminal voltage is greater than the cut-off voltage 3.65 V, the testing procedure goes to **e)**, else goes to **d)**; **d)**. rest for 600 s, then go to **c)**; **e)**. end test.

On the contrary, the battery is discharged by following steps: **A).** the C-rate of the battery is 0.5 C with CC discharged method for 300 s, if the terminal voltage is less than the cut-off voltage 2.2 V, the testing procedure goes to **C)**, else goes to **B)**; **B)**. rest for 3600 s, then go to **A)**; **C).** low current with 0.04 C that continuously discharges 300 s, if the terminal voltage is less than the cut-off voltage 2.2 V, the testing procedure goes to **E)**, else goes to **D)**; **D)**. rest for 600 s, then go to **C)**; **E)**. end test. Fig.3(c) indicates the charged and discharged profiles of OCV test combined incremental current

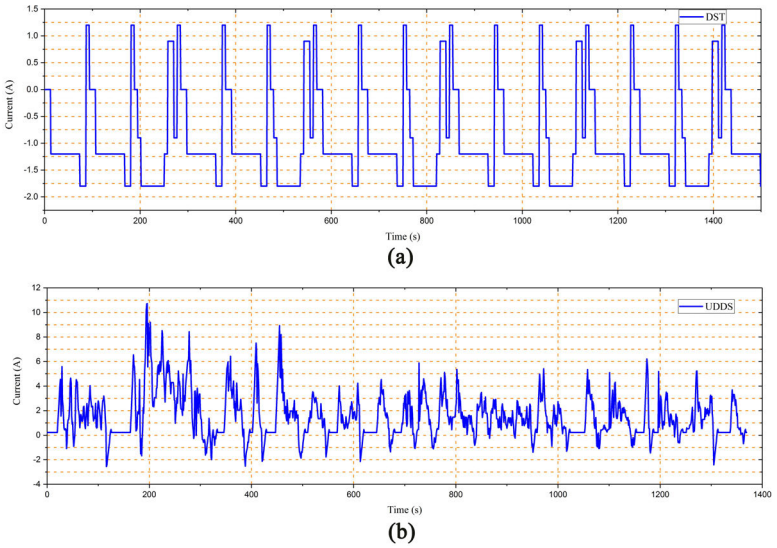

FIGURE 5. Battery testing driving cycle: (a) Current profile of dynamic stress test (DST); (b) Urban Dynamometer Driving Schedule (UDDS).

with low current tests at 25°C. Lastly, we can respectively fit OCV-SoC polynomial function by Eq. (2) using the OCV voltage data of the test at corresponding SoC of the charged and discharged processes.

E. OCV-SoC CURVES OF THREE OCV TESTS

The Fig.4 gives a clear indication that the OCV-SoC curves of three OCV tests at different temperatures (5°C, 25°C, 40°C) will vary markedly during the charged or the discharged process. The OCV-SoC curves of three OCV tests in the entire process initially increase between 0% SoC and 10% SoC, then there is a barely discernible change from 10% SoC to 90% SoC, finally, the OCV-SoC curves endure a consistent upward surge in the last phase. There is an obvious difference between the charged OCV-SoC curve and the discharged OCV-SoC curve at every OCV test, which is informed by observing the Fig.4 (A), (B) and (C). This difference is caused by the OCV hysteresis phenomenon [32], [33], which is the change of the volume and the structure of $LiFePO_4$ crystal due to Li^+ is inserted or released into the $LiFePO_4$ crystal during the charged or discharged processes [32], [34], [35].

The more overlap between the charged OCV-SoC curve and the discharged OCV-SoC curve in each OCV test, the lower influence of the OCV hysteresis phenomenon and the better choice of the OCV test will have. Therefore, according to the OCV hysteresis phenomenon, we can conclude the method which combines incremental with low current OCV test (red lines) performs better than the incremental OCV test (blue lines) and the low current OCV test (green lines) at three temperatures (5°C, 25°C, 40°C) in the Fig.4. The OCV-SoC polynomial coefficient through Eq. (2) using the OCV data of each OCV test at corresponding SoC of the charged or discharged processes are fitted.

IV. METHODOLOGY OF SoC ONLINE ESTIMATION AND RELIABILITY COMPARISON

A. AEKF FOR SoC ONLINE ESTIMATION

Kalman filter (KF) algorithm is a method for the SoC online estimation that depends on the reliable battery equivalent circuit model and the accuracy parameters identification of the battery model. However, KF only suits for the linear system. In order to extend to the complex nonlinear system, the extended Kalman filter (EKF) algorithm is proposed by using the Taylor expansion, which may lead to truncation errors and result in the EKF is divergent at some initial SoC value [37,38]. In addition, EKF assumes that the noise in the battery model is invariable, which does not conform to the reality. Therefore, the adaptive extended Kalman filter (AEKF) algorithm is employed to solve the noise statistical characteristics in the filtering algorithm, it can adaptively update as the estimation results change.

For the AEKF, the dispersed state-space equation of the DP battery model can be shown as:

$$\begin{cases} x(k) = f(x_{k-1}, u_{k-1}) + w_{k-1} \\ = A \cdot x(k-1) + B \cdot u(k-1) + w_{k-1} \\ y(k) = h(x_k, u_k) + v_k = C \cdot x(k) + D \cdot u(k) + v_k \end{cases} \tag{13}$$

where the state variables are

$$x(k) = [SoC(k)\ U_1(k)\ U_2(k)]^T$$

The system excitation is $u(k) = I(k)$

The measured variable is $y(k) = U_t(k)$

w_k and v_k respectively represent the process noise and the measurement noise that both have zero-mean. The coefficient

TABLE 2. AEKF for SoC online estimation process.

Step 1: Initialization	Set the initial value: x_0, P_0, Q_0, R_0
Step 2: Prior estimation (obtained SoC prior value)	State prior estimation: $x_k^f = f\left(x_{k-1}, u_{k-1}\right)$
	Error covariance matrix: $P_k^f = A_{k-1}P_{k-1}A_{k-1}^T + Q_{k-1}$
Step 3: Obtained OCV	$OCV = k_0 + k_1SoC + k_2SoC^2 + k_3SoC^3 + k_4SoC^4 + k_5SoC^5 + k_6SoC^6 + k_7SoC^7 + k_8SoC^8 + k_9SoC^9$
Step 4: Measured terminal voltage	y_k
Step 5:Voltage error matrix	$e_k = y_k - h\left(x_k^f, u_k\right)$
Step 6: Posteriori estimation, then go to Step 2, loop between Step 2 and Step 6	Kalman gain matrix: $G_k = P_k^f C_k^T \left(C_k P_k^f C_k^T + R_{k-1}\right)^{-1}$
	Adaptive noise covariance matching: $\begin{cases} H_k = \dfrac{1}{M}\displaystyle\sum_{i=k-M+1}^{k} e_i e_i^T \\ R_k = H_k - C_k P_k^f C_k^T \\ Q_k = G_k H_k G_k^T \end{cases}$
	State modified: $x_k^b = x_k^f + G_k e_k$
	Error covariance matrix modified: $P_k^b = \left(I - G_k C_k\right) P_k^f$
Step 7: Estimation result	Real-time SoC value

matrix is described as:

$$A = \begin{bmatrix} 1 & 0 & 0 \\ 0 & e^{-\frac{T}{\tau_1}} & 0 \\ 0 & 0 & e^{\frac{T}{\tau_2}} \end{bmatrix}, \quad B = \begin{bmatrix} -\dfrac{T}{Q_n} \\ R_1 \cdot (1 - e^{\frac{T}{\tau_1}}) \\ R_2 \cdot (1 - e^{\frac{T}{\tau_2}}) \end{bmatrix},$$

$$C = \begin{bmatrix} \dfrac{U_{oc}(SoC(k))}{SoC(k)} - 1 - 1 \end{bmatrix}, \quad D = -R_0.$$

The detailed process of SoC online estimation using AEKF is shown in Table 2.

Where P is the state error covariance matrix, Q and R are the process noise covariance matrix and the measured noise covariance matrix, respectively. H is the terminal voltage error covariance matrix based on the moving window function, M is the size of window about moving window function, G is the Kalman gain matrix, e is voltage error matrix, x_k^f and P_k^f represent the state prior estimation value and the error covariance matrix of the prior estimation, respectively, x_k^b and P_k^b represent the state posteriori estimation value and the error covariance matrix of the posteriori estimation, respectively.

B. RELIABILITY COMPARISON OF SoC ONLINE ESTIMATION BETWEEN AEKF AND EKF

There is a dynamic test method simulated the real driving cycle of the EV to obtain the reliable assessment of the BMS core algorithm. The DST is one of the most common dynamic tests to acquire the performance of the battery. The driving cycle of DST is converted from the time-velocity profile of the EV through the Advisor software. The current profile of DST consisted of an intact time cycle is indicated in Fig.5(a). Firstly, the FRLS is employed to execute the parameters online identification of the fresh LFP battery at 25°C under the DST test, the real-time value of parameters is demonstrated in Fig.6. The ohmic resistance R_0 of DP battery model, concentration polarization resistance R_1, concentration polarization capacitance C_1, electrochemical polarization resistance R_2, and electrochemical polarization capacitance C_2 are respectively shown in Fig.6 (a)-(e). Next, in order to get an optimal selection of the SoC online estimation, we carry out the reliability comparison between AEKF and EKF at 25°C under the DST test. The OCV-SoC relationship curve is applied to the AEKF and the EKF SoC online estimation, which is both fitted through the OCV test which combines incremental with low current OCV test.

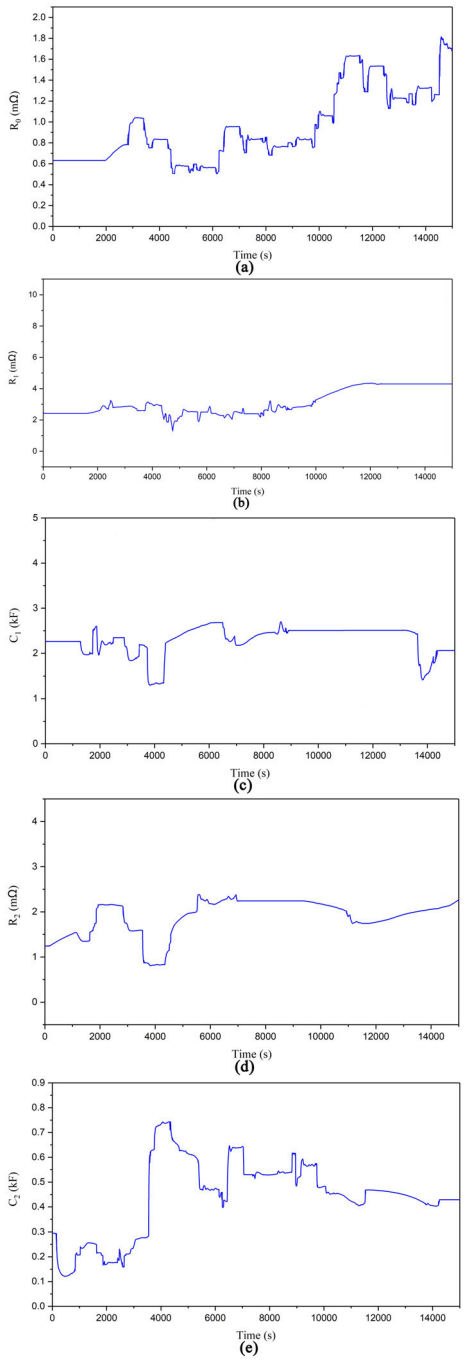

FIGURE 6. Results of parameters identification for DST test at 25°C: (a) R_0, (b) R_1, (c) C_1, (d) R_2, (e) C_2.

The initial SoC values of both AEKF and EKF have an impact on the robustness of the algorithm, therefore, we simultaneously set the initial SoC value equals to 70% (have 30% initial error) for AEKF and EKF. The fully charged battery is 100% SoC, and the true SoC can be calculated by using the ampere hour counting method. Real SoC online estimation values and SoC errors between AEKF and EKF for DST test at 25°C are respectively shown in Fig.7(a). By observing the Fig.7(a)-(i), the AEKF curve can approach the true SoC curve very well under the condition that the initial SoC is incorrect, but the EKF curve cannot. Meanwhile, the Fig.7(a)-(ii) demonstrates the obvious SoC errors between AEKF and EKF over the DST driving cycle. The SoC error of EKF falls consistently from 30% SoC error to 2% SoC error, however, the AEKF has less than 2% SoC error with small fluctuations during the entire test. Therefore, the robustness of the AEKF algorithm for SoC online estimation is better than the EKF. In order to verify the accuracy of the AEKF and the EKF, comparisons of terminal voltage values and the corresponding errors between AEKF and EKF for DST test at 25°C are indicated in Fig.7(b). Fig.7(b)-(i) reveals that the terminal voltage curve of AEKF algorithm accurately tracks the true measured voltage curve very well, which is better than EKF algorithm. The absolute terminal voltage errors of AEKF algorithm are below 0.5%, however, majority of the terminal voltage errors about EKF algorithm exceed 0.5%, which can be indicated in Fig.7(b)-(ii). From Fig.7, with the SOC errors decreasing, the terminal voltage errors increasing, this is due to the effect of electrochemical polarization and concentration polarization inside the battery makes the battery voltage rebound during the end of DST test. The above-mentioned analysis makes clear that the accuracy of the AEKF algorithm for SoC online estimation is superior to the EKF. According to the comparison results of the robustness and the accuracy between AEKF and EKF for SoC online estimation under the DST test at 25°C, we choose the AEKF algorithm for SoC estimation to conduct the research in next section.

V. RESULTS AND DISCUSSION

Based on previous section, the AEKF algorithm as the optimal SoC online estimation method is selected, we conduct the research scheme whether the different OCV tests have an effect on the SoC online estimation at various temperatures modes and the complicated driving cycle. The SoC online estimator of the OCV-SoC relationship curve fitted by the low current OCV test is named as the LO estimator, the same naming principle is applied to other estimators, respectively are the IO estimator and the CIL estimator. Test temperatures include the low temperature 5°C, the room temperature 25°C, the high temperature 40°C, respectively. Compared with the DST test, the UDDS possesses the more complex driving schedule which can adequately verify the proposed SoC online estimation. Meanwhile, on the premise of no influence it filters actual driving cycle tests data according to certain specifications to implement the propose of scaled-down the current profile of the UDDS, because the battery cannot take a risk of high currents which may trigger the thermal runaway [38]. The scaled-down current profile of UDDS is shown in Fig.5 (b), which takes into account the regenerative braking charging due to it is the property of real driving cycle of the EV [39]. The BMS of the EV for the SoC estimation should have adaptive abilities when the initial SoC is incorrect. In order to verify the convergence speed and robustness among the three estimators, the research setting

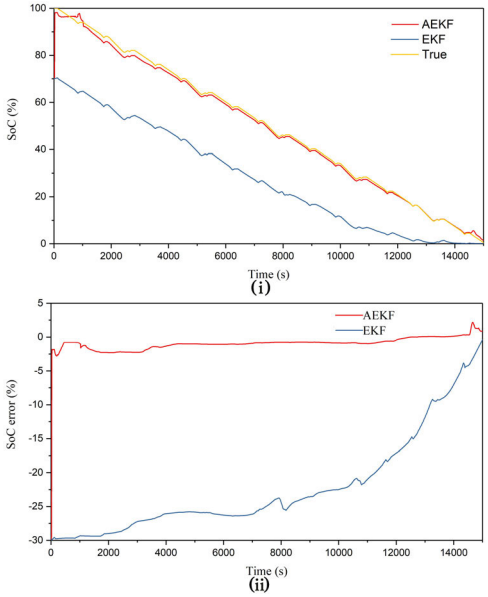

(a) Results of SoC online estimation between AEKF and EKF for DST test at 25°C: (i) SoC values, (ii) SoC error.

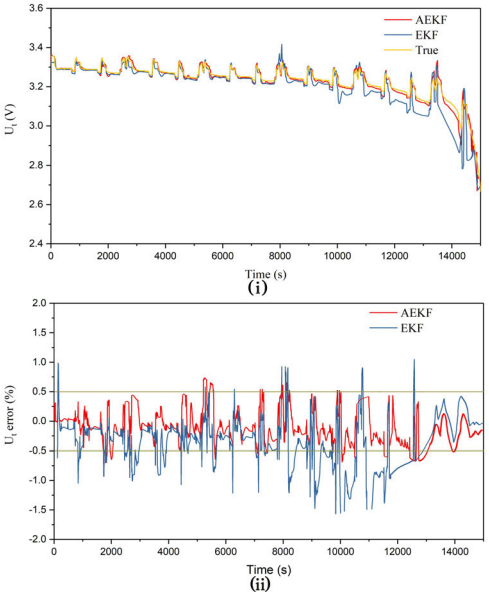

(b) Terminal voltage values of SoC online estimation between AEKF and EKF for DST test at 25°C:(i) terminal voltage, (ii) terminal voltage error.

FIGURE 7. Reliability comparison of SoC online estimation between AEKF and EKF.

the initial SoC is 70% that has 30% SoC error. The root mean square error (RMSE) and the mean absolute error (MAE) are two statistical criterions to evaluate the error performance between three estimators about the real SoC online estimation values and true SoC values. Equations of the RMSE and the MAE are defined as follows:

$$RMSE = \sqrt{\frac{\sum_{i=1}^{k} |A_T - A_M|}{k}}, \quad MAE = \frac{1}{k}\sum_{i=1}^{k} |A_T - A_M| \tag{14}$$

where k is sampled points, A_T and A_M respectively represent the true SoC values via the ampere hour counting method and the SoC estimated values by using three estimators.

The comparative results of SoC estimated values among three estimators at the room temperature 25°C by using UDDS testing data are indicated in Fig.8. For the Fig.8 (i), it can be seen that all of the three estimators can quickly converge to the true SoC values under the condition of an incorrect initial SoC value. Moreover, except for the last phase, the curves of the three estimators overlap in most areas that can be observed in the zoom figure of the Fig.8 (i). Further research shows that the corresponding SoC errors of three estimators are below 1%, the SoC error of the CIL estimator is smaller than that of both the LO estimator and the IO estimator, which can be revealed in Fig.8 (ii). To fully illustrate the SoC online estimation accuracy of the three estimators, the MAE and the RMSE are respectively calculated to act as the standard of the model performance and the index of fitting of the model. As shown in Fig.8 (iii), the RMSE of the CIL estimator is 0.7617% and the MAE of the CIL estimator is 0.7480%, which is respectively less than that of

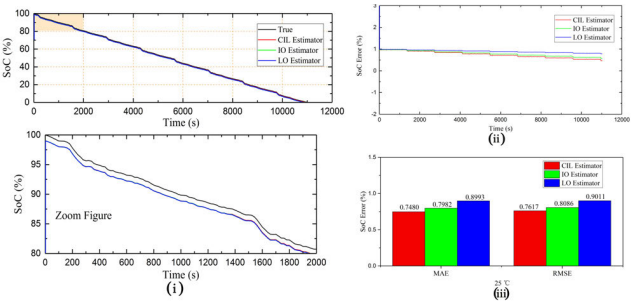

FIGURE 8. Comparative results of three SoC estimators under UDDS test at 25°C.

both the LO estimator and the IO estimator. In addition, the estimated terminal voltages of the three estimators can track well with the true measured voltages based on the UDDS testing data at 25°C, as shown in Fig.9 (i). Fig.9 (ii) describes the situation that the estimated terminal voltage errors of the CIL estimator, the IO estimator and the LO estimator all remain low at roughly the same level during the entire testing process. However, the estimated terminal voltage errors of the CIL estimator are less than that of the other two estimators by careful observation. The comparison results of both estimated SoC values and estimated terminal voltages declare that the CIL estimator performs better than the IO estimator and the LO estimator at 25°C under the UDDS test.

The high temperature is a common working environment for the EV, it is important for the EV to explore the accuracy of the SoC estimation during realistic driving cycles. In terms of the complex UDDS driving cycle, Fig.10 depicts results of

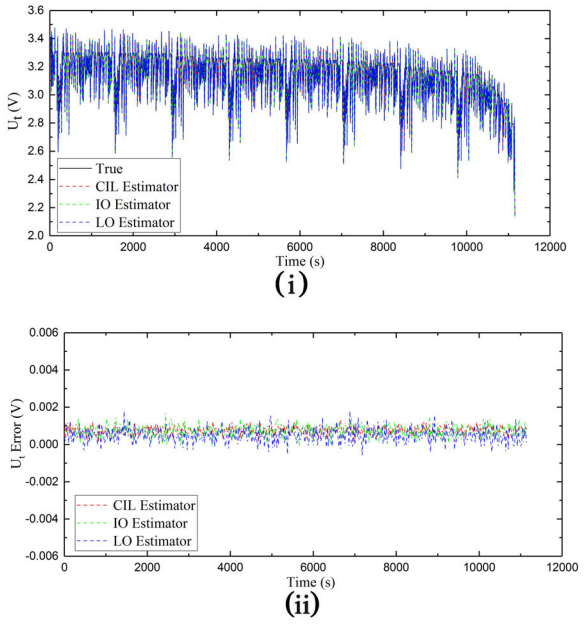

FIGURE 9. Comparisons of measured voltage and estimated voltage under UDDS test at 25°C.

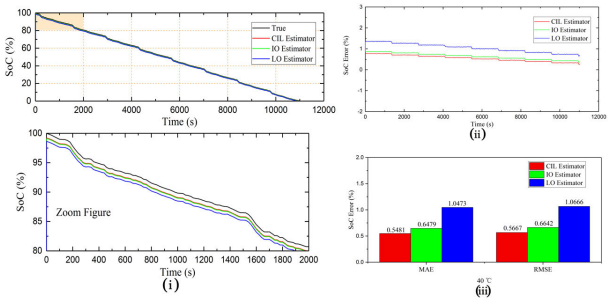

FIGURE 10. Comparative results of three SoC estimators under UDDS test at 40°C.

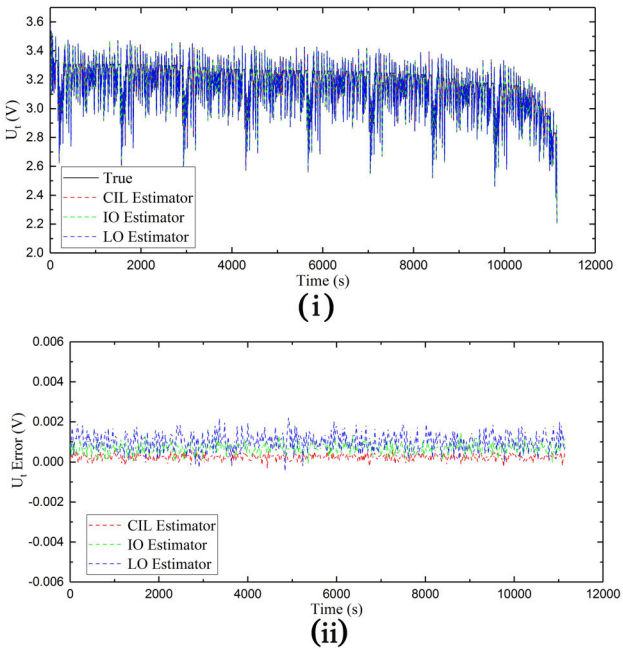

FIGURE 11. Comparisons of measured voltage and estimated voltage under UDDS test at 40°C.

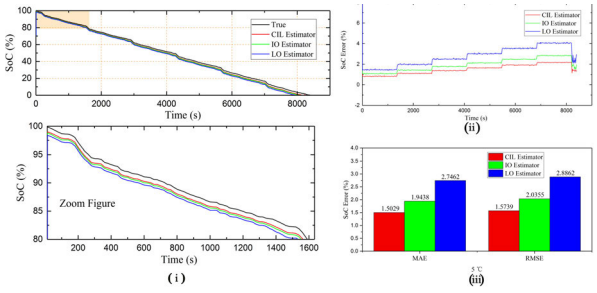

FIGURE 12. Comparative results of three SoC estimators under UDDS test at 5°C.

three SoC estimators at 40°C under this driving cycle. The phenomena of the fast convergence about three estimators under the condition of an incorrect initial SoC value are indicated in Fig.10 (i), the SoC estimated values of both the CIL estimator and the IO estimator are almost coincident, which are closer to the true SoC values than that of the LO estimator by investigating the zoom figure of the Fig.10 (i). The SoC curves of three estimators tend to approach the true SoC curve gradually, because the SoC errors of three estimators gradually decrease with the UDDS test, as shown in Fig.10(ii). What's more, the maximum SoC error of the CIL estimator is below 0.6%, which is much smaller than that of both the IO estimator and the LO estimator. The RMSE and the MAE of three estimators are illustrated in Fig.10 (iii), the RMSE of the CIL estimator, IO estimator and LO estimator respectively equals to 0.5667%, 0.6642% and 1.0666%. Similarly, the MAE of the CIL estimator, the IO estimator and the LO estimator respectively equals to 0.5481%, 0.6479% and 1.0473%. Fig.11 shows that the estimated terminal voltages of three estimators have proven to be well matched with the true measured voltages, however, the estimated terminal voltage of the CIL estimator has smaller fluctuation than that of the other two estimators. The conclusion can be obtained that the CIL estimator can better adapt to the high temperature than the IO estimator and the LO estimator.

It is well known that the use of the battery system is greatly affected by the ambient temperature. Especially at the low temperature, the decrease of the electrochemical reaction activity of the battery may result in the precipitation of the electrode Li^+, which impacts on the power characteristic of the battery. It is necessary to compare the SoC estimated accuracy of three estimators at low temperature 5°C by using the UDDS test. We can clearly distinguish the SoC estimated values of three estimators and the true SoC values via Fig.12(i). Contrastive analysis of SoC errors among three estimators are shown in Fig.12 (ii-iii). Fig.12 (ii) depicts that SoC errors of the CIL estimator is a situation of the sustained growth until the end of the UDDS driving cycles, similar

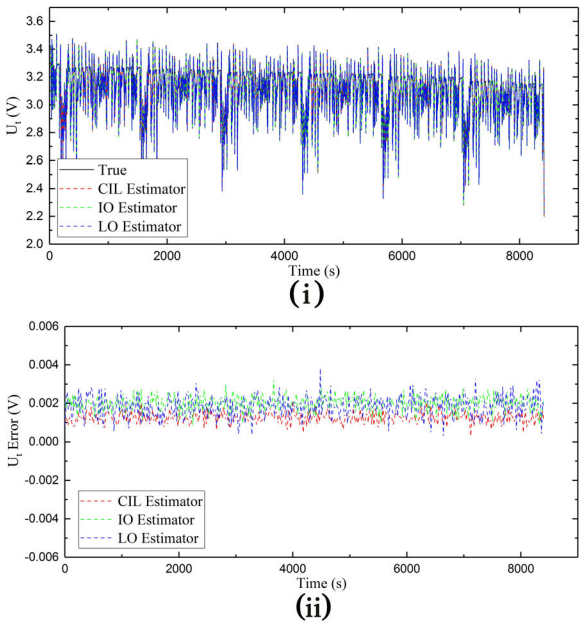

FIGURE 13. **Comparisons of measured voltage and estimated voltage under UDDS test at 5°C.**

patterns emerge in the IO estimator and the LO estimator. Overall, it is clear that the SoC errors of the CIL estimator is less than that of both the other two estimators. As mentioned in Fig.12 (iii), the RMSE and MAE of the CIL estimator are a lot better and more stable than that of the IO estimator and the LO estimator. Fig.13 describes the comparative results of both measured voltages and estimated voltages among three estimators under UDDS test at 5°C, the results show that the estimated voltage of the CIL estimator agrees well with the true measured voltages than that of the other two estimators. Although the three estimators estimate worse at 5°C than that at 25°C and 40°C during UDDS test, but the CIL estimator performs better than the IO estimator and the LO estimator at 5°C. One reason is that the precipitation of the electrode Li^+ can be potentially reduced via the low current of CIL OCV test at low temperature, which results in the improvement of the OCV-SoC relationship to compare with the IO OCV teat and the LO OCV test. Moreover, the interaction of the incremental low current with the relaxation time in the CIL OCV test makes the SoC estimated accuracy of the CIL estimator is higher than that of the other two estimators at 5°C, 25°C and 40°C.

VI. CONCLUSION

Different OCV test methods affect the correlation of the OCV-SoC, accordingly, an excellent OCV-SoC relationship can improve the convergence speed and the accuracy of the SoC online estimation. In this paper, we developed a DP battery model to address the parameters online identification of the battery model. The comparative analysis of the SoC estimation algorithm between the AEKF and EKF indicated that the AEKF had higher accuracy and better robustness of SoC estimation than that of the EKF under driving cycles. The OCV-SoC fitting relationship that respectively obtained from the CIL OCV test, the IO test and the LO test were applied in the AEKF algorithm of the SoC estimation. In the meantime, the UDDS driving cycles were run on the battery under various temperatures to verify the accuracy of the three SoC estimators. A comparison was executed among the three SoC estimators with regard to the influence of the corresponding OCV-SoC relationship for the SoC estimation. The study results illustrate that the CIL estimator performs better than the IO estimator and the LO estimator, which take into account the various changes of OCV testing temperature. Therefore, the CIL estimator is the most recommended SoC estimation to load in the BMS for the EV, which can not only prevent the over-charge and over-discharge of batteries but also provide accurate driving ranges of the EV.

Under the current work scope and the limited time of this research, the scenarios of three OCV tests for affecting on SoC online estimation were all studied at above 0°C. However, further work will be required to identify whether the OCV test at below 0°C has a huge influence on the SoC online estimation. Furthermore, state observers of the battery module that contain the state of charge, the state of power, and the state of health, which will be explored in our future work. Meanwhile, we will launch two potential applications with the proposed data processing for online estimation. The one is the online estimation of the battery management system (BMS) for electric vehicles, the other is present a framework for estimating the life cycle cost of storage application about standalone power systems. Also, there have other potential applications with the proposed data processing for online estimation, which is employed to engineering applications that take more factors into consideration [40]–[44].

REFERENCES

[1] Y. Wang, G. Zhou, T. Li, and X. Wei, "Comprehensive evaluation of the sustainable development of battery electric vehicles in China," *Sustainability*, vol. 11, no. 20, p. 5635, Oct. 2019.

[2] Z. Bi, T. Kan, C. C. Mi, Y. Zhang, Z. Zhao, and G. A. Keoleian, "A review of wireless power transfer for electric vehicles: Prospects to enhance sustainable mobility," *Appl. Energy*, vol. 179, pp. 413–425, Oct. 2016.

[3] X. Hu, C. Zou, C. Zhang, and Y. Li, "Technological developments in batteries: A survey of principal roles, types, and management needs," *IEEE Power Energy Mag.*, vol. 15, no. 5, pp. 20–31, Sep. 2017.

[4] M. Hannan, M. Lipu, A. Hussain, and A. Mohamed, "A review of lithium-ion battery state of charge estimation and management system in electric vehicle applications: Challenges and recommendations," *Renew. Sustain. Energy Rev.*, vol. 78, pp. 834–854, Oct. 2017.

[5] C. Wang, R. Yang, and Q. Yu, "Wavelet transform based energy management strategies for plug-in hybrid electric vehicles considering temperature uncertainty," *Appl. Energy*, vol. 256, Dec. 2019, Art. no. 113928.

[6] Y. Wang, Q. Gao, G. Wang, P. Lu, M. Zhao, and W. Bao, "A review on research status and key technologies of battery thermal management and its enhanced safety," *Int. J. Energy Res.*, vol. 42, no. 13, pp. 4008–4033, Oct. 2018.

[7] Z. Li, J. Huang, B. Y. Liaw, and J. Zhang, "On state-of-charge determination for lithium-ion batteries," *J. Power Source*, vol. 348, pp. 281–301, Apr. 2017.

[8] P. Křivík, "Methods of SoC determination of lead acid battery," *J. Energy Storage*, vol. 15, pp. 191–195, Feb. 2018.

[9] P. Křivík, S. Vaculík, P. Bača, and J. Kazelle, "Determination of state of charge of lead-acid battery by EIS," *J. Energy Storage*, vol. 21, pp. 581–585, Feb. 2019.

[10] R. Xiong, F. Sun, X. Gong, and C. Gao, "A data-driven based adaptive state of charge estimator of lithium-ion polymer battery used in electric vehicles," *Appl. Energy*, vol. 113, pp. 1421–1433, Jan. 2014.
[11] Z. Deng, L. Yang, Y. Cai, H. Deng, and L. Sun, "Online available capacity prediction and state of charge estimation based on advanced data-driven algorithms for lithium iron phosphate battery," *Energy*, vol. 112, pp. 469–480, Oct. 2016.
[12] R. Xiong, J. Cao, Q. Yu, H. He, and F. Sun, "Critical review on the battery state of charge estimation methods for electric vehicles," *IEEE Access*, vol. 6, pp. 1832–1843, 2018.
[13] M. Mastali, E. Samadani, S. Farhad, R. Fraser, and M. Fowler, "Three-dimensional multi-particle electrochemical model of $LiFePO_4$ cells based on a resistor network methodology," *Electrochim. Acta*, vol. 190, pp. 574–587, Feb. 2016.
[14] E. Hosseinzadeh, R. Genieser, D. Worwood, A. Barai, J. Marco, and P. Jennings, "A systematic approach for electrochemical-thermal modelling of a large format lithium-ion battery for electric vehicle application," *J. Power Source*, vol. 382, pp. 77–94, Apr. 2018.
[15] X. Lai, W. Gao, Y. Zheng, M. Ouyang, J. Li, X. Han, and L. Zhou, "A comparative study of global optimization methods for parameter identification of different equivalent circuit models for Li-ion batteries," *Electrochim. Acta*, vol. 295, pp. 1057–1066, Feb. 2019.
[16] N. Tian, Y. Wang, and J. Chen, "On parameter identification of an equivalent circuit model for lithium-ion batteries," in *Proc. IEEE Conf. Control Technol. Appl. (CCTA)*, Mauna Lani, HI, USA, Aug. 2017, pp. 187–192.
[17] Z. Wei, S. Meng, B. Xiong, D. Ji, and K. J. Tseng, "Enhanced online model identification and state of charge estimation for lithium-ion battery with a FBCRLS based observer," *Appl. Energy*, vol. 181, pp. 332–341, Nov. 2016.
[18] T. Feng, L. Yang, X. Zhao, H. Zhang, and J. Qiang, "Online identification of lithium-ion battery parameters based on an improved equivalent-circuit model and its implementation on battery state-of-power prediction," *J. Power Source*, vol. 281, pp. 192–203, May 2015.
[19] L. Zheng, J. Zhu, G. Wang, D. D.-C. Lu, and T. He, "Differential voltage analysis based state of charge estimation methods for lithium-ion batteries using extended Kalman filter and particle filter," *Energy*, vol. 158, pp. 1028–1037, Sep. 2018.
[20] S. Habbachi, M. Sayadi, and N. Rezzoug, "Partical filtering for orientation determining using inertial sensors IMU," in *Proc. 4th Int. Conf. Adv. Technol. Signal Image Process. (ATSIP)*, Sousse, Tunisia, Mar. 2018, pp. 1–5.
[21] L. Wang, D. Lu, Q. Liu, L. Liu, and X. Zhao, "State of charge estimation for $LiFePO_4$ battery via dual extended Kalman filter and charging voltage curve," *Electrochim. Acta*, vol. 296, pp. 1009–1017, Feb. 2019.
[22] Y. Shen, "Adaptive extended Kalman filter based state of charge determination for lithium-ion batteries," *Electrochim. Acta*, vol. 283, pp. 1432–1440, Sep. 2018.
[23] J.-N. Shen, Y.-J. He, Z.-F. Ma, H.-B. Luo, and Z.-F. Zhang, "Online state of charge estimation of lithium-ion batteries: A moving horizon estimation approach," *Chem. Eng. Sci.*, vol. 154, pp. 42–53, Nov. 2016.
[24] F. Zheng, Y. Xing, J. Jiang, B. Sun, J. Kim, and M. Pecht, "Influence of different open circuit voltage tests on state of charge online estimation for lithium-ion batteries," *Appl. Energy*, vol. 183, pp. 513–525, Dec. 2016.
[25] C. Lin, Q. Yu, R. Xiong, and L. Y. Wang, "A study on the impact of open circuit voltage tests on state of charge estimation for lithium-ion batteries," *Appl. Energy*, vol. 205, pp. 892–902, Nov. 2017.
[26] X. Lai, Y. Zheng, and T. Sun, "A comparative study of different equivalent circuit models for estimating state-of-charge of lithium-ion batteries," *Electrochim. Acta*, vol. 259, pp. 566–577, Jan. 2018.
[27] Q. Q. Yu, R. Xiong, L. Y. Wang, and C. Lin, "A comparative study on open circuit voltage models for Lithium-ion batteries," *Chin. J. Mech. Eng.*, vol. 31, no. 4, pp. 651–658, 2018.
[28] G. L. Plett, "Extended Kalman filtering for battery management systems of LiPB-based HEV battery packs," *J. Power Source*, vol. 134, no. 2, pp. 252–261, Aug. 2004.
[29] K. Sarrafan, K. Muttaqi, and D. Sutanto, "Real-time estimation of model parameters and state-of-charge of lithiumion batteries in electric vehicles using recursive least-square with forgetting factor," in *Proc. IEEE Int. Conf. Power Electron., Drives Energy Syst. (PEDES)*, Chennai, India, Dec. 2018, pp. 1–6.
[30] Y. Xing, W. He, M. Pecht, and K. L. Tsui, "State of charge estimation of lithium-ion batteries using the open-circuit voltage at various ambient temperatures," *Appl. Energy*, vol. 113, pp. 106–115, Jan. 2014.
[31] B. Li and S. Bei, "Estimation algorithm research for lithium battery SOC in electric vehicles based on adaptive unscented Kalman filter," *Neural Comput. Appl.*, vol. 31, no. 12, pp. 8171–8183, Dec. 2019.
[32] G. Dong, J. Wei, C. Zhang, and Z. Chen, "Online state of charge estimation and open circuit voltage hysteresis modeling of $LiFePO_4$ battery using invariant imbedding method," *Appl. Energy*, vol. 162, pp. 163–171, Jan. 2016.
[33] F. Feng, R. Lu, G. Wei, and C. Zhu, "Online estimation of model parameters and state of charge of $LiFePO_4$ batteries using a novel open-circuit voltage at various ambient temperatures," *Energies*, vol. 8, no. 4, pp. 2950–2976, Apr. 2015.
[34] Y. Li, F. Qi, H. Guo, Z. P. Guo, M. Y. Li, and W. L. Wu, "Characteristic investigation of an electrochemical-thermal coupled model for a Li $FePO_4$/graphene hybrid cathode lithium-ion battery," *Case Stud. Therm. Eng.*, vol. 13, Mar. 2019, Art. no. 100387.
[35] J. Lim, Y. Li, D. H. Alsem, H. So, S. C. Lee, P. Bai, D. A. Cogswell, X. Liu, N. Jin, Y.-S. Yu, N. J. Salmon, D. A. Shapiro, M. Z. Bazant, T. Tyliszczak, and W. C. Chueh, "Origin and hysteresis of lithium compositional spatiodynamics within battery primary particles," *Science*, vol. 353, no. 6299, pp. 566–571, Aug. 2016.
[36] W. Waag, C. Fleischer, and D. U. Sauer, "Critical review of the methods for monitoring of lithium-ion batteries in electric and hybrid vehicles," *J. Power Source*, vol. 258, pp. 321–339, Jul. 2014.
[37] H. Pan, Z. Lü, W. Lin, J. Li, and L. Chen, "State of charge estimation of lithium-ion batteries using a grey extended Kalman filter and a novel open-circuit voltage model," *Energy*, vol. 138, pp. 764–775, Nov. 2017.
[38] Y. Li, F. Qi, H. Guo, Z. Guo, G. Xu, and J. Liu, "Numerical investigation of thermal runaway propagation in a Li-ion battery module using the heat pipe cooling system," *Numer. Heat Transf., A, Appl.*, vol. 75, no. 3, pp. 183–199, Feb. 2019.
[39] R. Maia, M. Silva, R. Araújo, and U. Nunes, "Electrical vehicle modeling: A fuzzy logic model for regenerative braking," *Expert Syst. Appl.*, vol. 42, no. 22, pp. 8504–8519, Dec. 2015.
[40] S. Li, L. Li, Z. Li, X. Chen, T. Fernando, H. H.-C. Iu, G. He, Q. Wang, and X. Liu, "Event-trigger heterogeneous nonlinear filter for wide-area measurement systems in power grid," *IEEE Trans. Smart Grid*, vol. 10, no. 3, pp. 2752–2764, May 2019.
[41] Y. Yu, Z. Li, X. Liu, K. Hirota, X. Chen, T. Fernando, and H. H. C. Iu, "A nested tensor product model transformation," *IEEE Trans. Fuzzy Syst.*, vol. 27, no. 1, pp. 1–15, Jan. 2019.
[42] X. Liu, L. Li, Z. Li, X. Chen, T. Fernando, H. H.-C. Iu, and G. He, "Event-trigger particle filter for smart grids with limited communication bandwidth infrastructure," *IEEE Trans. Smart Grid*, vol. 9, no. 6, pp. 6918–6928, Nov. 2018.
[43] B. Liu, Z. Li, X. Chen, Y. Huang, and X. Liu, "Recognition and vulnerability analysis of key nodes in power grid based on complex network centrality," *IEEE Trans. Circuits Syst. II, Exp. Briefs*, vol. 65, no. 3, pp. 346–350, Mar. 2018.
[44] S. Li, Y. Hu, L. Zheng, Z. Li, X. Chen, T. Fernando, H. H. C. Iu, Q. Wang, and X. Liu, "Stochastic event-triggered cubature Kalman filter for power system dynamic state estimation," *IEEE Trans. Circuits Syst. II, Exp. Briefs*, vol. 66, no. 9, pp. 1552–1556, Sep. 2019.

YUAN LI received the M.Sc. degree in mechnical engineering from the Inner Mongolia University of Technology, Hohhot, China, in 2016, where he is currently pursuing the Ph.D. degree.

Since December 2019, he has been a Visiting Researcher with the KTH Royal Institute of Technology, Sweden. His research focus on the battery management system (BMS) of the electric vehicle and energy storage. His current areas of active research, including the estimations of state of charge, state of health, and remaining useful life about lithium-ion battery systems.

HAO GUO (Member, IEEE) received the Ph.D. degree in mathematics from the Harbin Institute of Technology, Harbin, China, in 2012. He is currently an Associate Professor with the Jiangsu Provincial Key Laboratory of Advanced Robotics, Robotics and Microsystems Center, Soochow University, Suzhou, China. His research interests include human–computer interaction and intelligent system design for rehabilitation robot.

FEI QI (Member, IEEE) received the Ph.D. degree in engineering mechanics from the Center for Composite Materials, Harbin Institute of Technology, Harbin, China, in 2013. She is currently an Associate Professor with the School of Mechanical Engineering, Soochow University, Suzhou, China. Her research interests include structural analysis and the evaluation of high performance composite materials.

ZHIPING GUO received the B.S. degree in internal combustion engine from the China Agricultural University, Beijing, China, in 1981, and the M.Sc. degree in mechanical engineering from the Tsinghua University, Beijing, in 2003.

He is currently a Professor with the Inner Mongolia University of Technology. He has published over 30 articles and holds nine invention patents. His research interests include internal combustion engine working process, micro power and pneumatic machinery, and energy management of electric vehicle.

MEIYING LI received the B.S. degree in vehicle engineering from Nanjing Forestry University, Jiangsu, China, in 2017. She is currently pursuing the M.S. degree in mechanical engineering with the Inner Mongolia University of Technology, Hohhot, China.

Her research interests include development and application of energy management system of electric vehicle.